Errors and Uncertainties in Microwave Link Rainfall Estimation Explored Using Drop Size Measurements and High-Resolution Radar Data

HIDDE LEIJNSE* AND REMKO UIJLENHOET

Hydrology and Quantitative Water Management Group, Wageningen University, Wageningen, Netherlands

ALEXIS BERNE

Environmental Remote Sensing Laboratory, Swiss Federal Institute of Technology (EPFL), Lausanne, Switzerland

(Manuscript received 25 November 2009, in final form 29 April 2010)

ABSTRACT

Microwave links can be used for the estimation of path-averaged rainfall by using either the path-integrated attenuation or the difference in attenuation of two signals with different frequencies and/or polarizations. Link signals have been simulated using measured time series of raindrop size distributions (DSDs) over a period of nearly 2 yr, in combination with wind velocity data and Taylor's hypothesis. For this purpose, Taylor's hypothesis has been tested using more than 1.5 yr of high-resolution radar data. In terms of correlation between spatial and temporal profiles of rainfall intensities, the validity of Taylor's hypothesis quickly decreases with distance. However, in terms of error statistics, the hypothesis is seen to hold up to distances of at least 10 km. Errors and uncertainties (mean bias error and root-mean-square error, respectively) in microwave link rainfall estimates due to spatial DSD variation are at a minimum at frequencies (and frequency combinations) where the power-law relation for the conversion to rainfall intensity is close to linear. Errors generally increase with link length, whereas uncertainties decrease because of the decrease of scatter about the retrieval relations because of averaging of spatially variable DSDs for longer links. The exponent of power-law rainfall retrieval relations can explain a large part of the variation in both bias and uncertainty, which means that the order of magnitude of these error statistics can be predicted from the value of this exponent, regardless of the link length.

1. Introduction

Microwave links have been shown to be highly suitable for estimating path-averaged rainfall intensity (Ruf et al. 1996; Rincon and Lang 2002; Holt et al. 2003; Rahimi et al. 2003, 2004; Minda and Nakamura 2005; Krämer et al. 2005; Upton et al. 2005; Grum et al. 2005; Messer et al. 2006; Leijnse et al. 2007a,b). This is due to the near linearity of the relationship between the variable measured by the link (the path-integrated attenuation) and the rainfall intensity at link frequencies around 35 GHz. The proximity of the measurements to the ground is an additional advantage with respect to other remote sensing techniques, such as weather radar (e.g., Berne et al. 2004a). The availability of dense networks of such links used for cellular communication (Messer et al. 2006; Leijnse et al. 2007b; Zinevich et al. 2008, 2009) over large portions of the earth's land surface could potentially be used to greatly improve global rainfall estimation. The fields of hydrology and meteorology as well as agriculture, traffic management, and climate modeling could benefit from this improvement.

Rainfall attenuates electromagnetic signals traveling through the atmosphere. The magnitude of this attenuation varies with the rainfall intensity, which makes it a suitable quantity for rainfall estimation. Differences between two signals (with differing frequencies and/or polarizations) traveling through the same rain can also be used for this purpose, as long as the attenuations experienced are significantly different. In this paper, both

* Current affiliation: Royal Netherlands Meteorological Institute, de Bilt, Netherlands.

Corresponding author address: Hidde Leijnse, Royal Netherlands Meteorological Institute, Wilhelminalaan 10, 3732 GK De Bilt, Netherlands.
E-mail: hidde.leijnse@knmi.nl

DOI: 10.1175/2010JHM1243.1

single- and dual-frequency links, with configurations involving both horizontal and vertical polarizations, are studied in a simulation framework.

To be able to use microwave links for the estimation of rainfall, a number of issues such as wet antenna attenuation, temporal sampling, power resolution, and raindrop size distribution (DSD) variability need to be resolved (see Leijnse et al. 2007a,b). The first three of these aspects have been studied by Leijnse et al. (2008). The main purpose of this paper is to characterize ''errors'' [mean bias error (MBE)] and ''uncertainties'' [bias-corrected root-mean-square error (RMSE)] associated with spatial rainfall variation, including DSD variability, as functions of link length and frequency. These errors and uncertainties are highly useful in many applications using data from microwave links. To optimally use data from networks of commercial microwave links for the creation of rainfall maps (Zinevich et al. 2008, 2009), it is necessary to have information regarding errors and uncertainties for links with different configurations.

In this paper, errors and uncertainties are quantified by simulating microwave link signals and ''true'' path-averaged rainfall intensities from measured DSDs. Time series of DSDs are transformed to range profiles by invoking Taylor's hypothesis with measured wind velocities.

Aydin and Daisley (2002) carried out extensive analyses of the effects of drop canting angles and oscillations on specific and differential attenuation at 35 GHz, as well as the effects of point-scale DSD variability for three different climates. They have shown that the effect of canting angles on specific attenuation is negligible and the effect on differential attenuation is limited. The effect of canting angles will therefore not be considered in this paper. The effect of DSD variations was shown to be important for both specific and differential attenuation measurements. Berne and Uijlenhoet (2007) have investigated the dependence of link-estimated rainfall intensities on the interplay of spatial variations in DSDs and the length of the link. Their analyses are based on simulations of profiles of exponential DSD (Marshall and Palmer 1948) parameters. These simulations were carried out using a parameterization of spatial DSD variability that is in turn based on a single intense Mediterranean event (Berne and Uijlenhoet 2005), where zero rainfall is not considered. The analyses presented in this paper are based on measured DSDs over a period of nearly 2 yr, including intermittency (i.e., dry periods) to provide climatological statistics.

FIG. 1. Map of the Netherlands with the locations at which the different datasets have been collected. The gray-shaded area is the radar umbrella (a 240° sector), with the selected radial indicated in white. Note that all indicated locations are within a circle with a radius of 30 km.

2. Data

Two types of data will be used for the analyses presented in this paper. A high-resolution radar dataset will be used to test Taylor's hypothesis. Two drop size datasets are used in this paper: one to derive microwave link rainfall retrieval relations and another to derive errors and uncertainties in microwave link rainfall estimates. Figure 1 shows the locations at which the different datasets have been collected. All of these locations are within 60 km of each other. In addition, the Netherlands has no significant topography. Overeem et al. (2009a,b) have shown that rainfall climatology shows little variation over this region. We will therefore assume that the climates at these locations are the same. This climate is temperate, with prevailing southwesterly winds. Mean annual rainfall varies between 790 and 850 mm within the region of interest, with little seasonal variation. Annual 24-h rainfall maxima generally occur between July and December, and annual 1-h rainfall maxima between June and September, mainly because of the larger influence of convective rainfall in the summer. For more details regarding the rainfall climatology of the Netherlands, see Schuurmans et al. (2007), Overeem et al. (2008, 2009a,b), and van de Beek et al. (2010b).

a. High-resolution radar

We have used more than 1.5 yr (1993–94) of high-resolution X-band radar data to test the validity of

Taylor's hypothesis for the analyses presented in this paper. The radar used was located in Delft, the Netherlands (see Fig. 1), and was operated by the International Research Centre for Telecommunications and Radar (IRCTR) of Delft University of Technology. It has a range resolution of 120 m and a temporal resolution of approximately 16 s. The azimuth resolution is 1.875°, corresponding to approximately 30 m at 1-km range and 330 m at 10-km range. A single radial of the total radar scan is used here to test the Taylor hypothesis (this radial is indicated in white in Fig. 1). It is approximately parallel to the predominant wind direction in the Netherlands, which is southwest. The radar data have been corrected for both clutter and attenuation. For an extensive description of the radar data and details regarding the selected radial, see Ligthart and Nieuwkerk (1990), Leijnse et al. (2008), and van de Beek et al. (2010a). Additional hourly 10-m wind data are available from the Rotterdam Airport meteorological station (see Fig. 1), which is located 6.5 km to the southwest of the radar.

b. Drop size distributions

In this paper, two independent DSD datasets are used. One dataset is used for the derivation of relations between specific attenuation k (dB km^{-1}) and rainfall intensity R (mm h^{-1}), and the other is used to generate profiles of DSDs. We have used two separate datasets for this to ensure that the retrieval relations used are independent of the data to which they are applied. Because of the (usually) limited sampling area or volume, obtaining statistically robust measurements of DSDs is a challenge (e.g., Tokay et al. 2005; Uijlenhoet et al. 2006). Despite these limitations, measurements made by disdrometers are still valuable and will be used here. Two types of disdrometers will be used in this study: one based on the filter paper technique and one based on the extinction of light.

1) The De Bilt filter paper dataset

During more than a year (1968 and the first few months of 1969), drop size distributions have been collected by Wessels (1972) and coworkers in De Bilt, the Netherlands (see Fig. 1). This has been done using an instrument based on the filter paper technique (e.g., Marshall and Palmer 1948) for the measurement of drop sizes. By transporting filter paper under an exposure slit with an area of 20 cm^2, arrival times and drop sizes have been derived using the sizes of the stains left behind by the raindrops on the filter paper. Drop size distributions have been derived from these data by taking time periods in which Wessels (1972) judged the properties (e.g., intensity, drop size distribution) of the rain to be relatively constant, leading to time intervals between 1 and 50 min, with a mean of 8 min and a median of 5 min.

In this manner, 446 drop size distributions with rainfall intensities above 0.1 mm h^{-1} have been recorded in this period. Because the instrument was not designed to be outside continuously, it has only been operated when rain was expected or just after the start of an event. This may slightly influence the statistics of the measured DSDs. However, Uijlenhoet (1999) has shown that the distribution of rainfall intensities derived from the disdrometer closely follows the climatological distribution for the Netherlands. The small sampling area (20 cm^2) may also influence these statistics, as the measurement time interval should be rather large to collect enough drops. The resulting mean number of drops on which the DSDs are based is approximately 850. As a consistency check, the rainfall intensity computed using the derived DSDs has been compared to that measured by a nearby rain gauge, yielding positive results (i.e., 7% relative bias and a correlation coefficient of 0.94 between intensities from the different instruments).

2) The CESAR 2DVD dataset

Drop size data have been collected using a 2D video disdrometer (2DVD; Schönhuber et al. 1994; Kruger and Krajewski 2002) at the Cabauw Experimental Site for Atmospheric Research (CESAR) site in Cabauw, the Netherlands (see Fig. 1 and Leijnse et al. 2010). Additional wind data were collected as 10-min averages at 200 m above the terrain in a 213-m-high meteorological tower that is part of the CESAR site. The dataset spans nearly 2 yr (642 days).

The 2DVD estimates drop sizes, fall velocities, and shapes through measurements of the extinction of light. Two sheets of light, located at a slight vertical distance, are transmitted horizontally and sampled with two line configurations of charge-coupled device (CCD) sensors. The shapes (and hence sizes) of the particles falling through the 100-cm^2 planes constructed in this way can then be determined by the number of CCD sensors that register a decrease in signal. The vertical velocity of the drop can be determined by the delay in signal between the two lines of CCD sensors. For additional details regarding the measurement principle of the 2DVD, the reader is referred to Schönhuber et al. (1994) and Kruger and Krajewski (2002).

Because some mismatching between the drop size and drop velocity measurements may occur (i.e., the velocity of one drop is assigned to another and vice versa), only those drops that have diameters D (mm) and velocities v (m s^{-1}) that fall within a $\pm 40\%$ band of a theoretical $v(D)$ relation are used, as was suggested by Kruger and Krajewski (2002) and Thurai and Bringi (2005). The

$v(D)$ relation given by Beard (1976) is used for this purpose.

In the present study, the focus is purely on liquid precipitation (i.e., rainfall). Therefore, all time periods that are within 10 min of simultaneous occurrences of snow and a temperature below 278.15 K (i.e., 5°C) are removed from the dataset. Both the occurrence of snow and temperature are determined by a nearby present weather sensor (HSS-PW402b, e.g., Sheppard and Joe 2000). In the remainder of this paper, this dataset will be referred to as the 2DVD dataset.

3. Methodology

a. Electromagnetic scattering

An electromagnetic signal traveling through rain is attenuated by raindrops in its path. Neglecting the effect of multiple scattering, the total attenuation (in dB) of the signal due to rain is the sum of all the attenuations caused by the individual raindrops, which depends on their extinction cross sections. The extinction cross section of a raindrop depends on its size, shape, orientation, temperature, and on the wavelength and polarization of the signal.

Computations of scattering of electromagnetic waves by particles of arbitrary shapes are carried out here by using Waterman's T-matrix method (e.g., Waterman 1965; Mishchenko et al. 1996). This method has been numerically implemented by Mishchenko (2000), whose code is freely available online (at http://www.giss.nasa.gov/~crmim/t_matrix.html). From the amplitude scattering matrix produced by this code, the extinction cross section Q_{ext} (mm^2; e.g., van de Hulst 1957) of a particle for both horizontally and vertically polarized waves can be computed. The frequency- and temperature-dependent complex refractive index of water that is needed for these computations is calculated using the relation given by Liebe et al. (1991). The shape of raindrops has been assumed to be oblate spheroidal, the axis ratio of which is a function of volume-equivalent drop diameter D (mm). Czekala et al. (1999) have shown that deviations from extinction cross sections computed for more realistic raindrop shapes are insignificant. The oblateness–diameter relation used here is that which relates the drop diameter to the average oblateness of oscillating drops proposed by Andsager et al. (1999). Aydin and Daisley (2002) have shown that the use of different relations (that do not take drop oscillations into account) may yield severe underestimations of rainfall when using differential attenuation at 35 GHz. The effect of temperature has been investigated by Leijnse (2007), and was found to be of minor influence for single-frequency links with frequencies above 10 GHz. We have assumed a constant temperature of 288.15 K (i.e., 15°C) in this paper.

b. Profiles of DSDs

For the study of the dependence of the performance of microwave links for the retrieval of rainfall intensities on the variability of DSDs along the link path, it is necessary to have profiles of DSDs (see Berne and Uijlenhoet 2007). In this paper, we generate these profiles using measured arrival times of raindrops and measured wind velocities at 200-m altitude. Taylor's hypothesis is then invoked to convert arrival times into distances along a path. This means that we assume that the only change in rainfall at a point is caused by advection of the rainfall field. In other words, it is assumed that the spatial rainfall field does not change when viewed in a Lagrangian coordinate system moving with the rainfall event. This means that the rainfall along a line in the direction of the advection velocity can be derived from the temporal evolution of rainfall at a point on that line according to

$$Y(x + \Delta x, t) = Y\left(x, t - \frac{\Delta x}{u}\right). \tag{1}$$

Here, $Y(x, t)$ is a rainfall variable such as the number of drops of a given size, x (m) is the position along the line, t (s) is the time, and u (m s^{-1}) is the magnitude of the advection velocity. For the computation of profiles of DSDs, we also assume that the wind direction is always parallel to the orientation of the link. The validity of these assumptions is tested in section 4 using high-resolution radar data. The resolution of the generated profiles is 250 m, which is a compromise between sampling enough drops per range cell and having a high enough spatial resolution to capture important spatial rainfall variations. The resulting mean sampling interval per DSD is 12.1 s.

The resulting profiles of DSDs that are used for simulation purposes in the remainder of this paper have a mean rainfall intensity of 0.67 mm h^{-1} (0.81 mm h^{-1} if only nonzero rainfall is considered). Of all 250-m bins, 83% have rainfall intensities below 1 mm h^{-1}, 98% below 5 mm h^{-1}, 99.4% below 10 mm h^{-1}, and 99.9% below 30 mm h^{-1}. An indication of the effect of sampling errors on measured DSDs can be obtained by simulating disdrometer measurements as suggested by Uijlenhoet et al. (2006). To simulate 2DVD measurements we have assumed a Marshall and Palmer (1948) DSD with $R = 0.81$ mm h^{-1} and a sampling interval of 12.1 s (the mean sampling interval in the 2DVD dataset). This yields (based on 2500 realizations) a coefficient of variation of R of 20% and 10% and 90% quantiles of R of 0.62 mm h^{-1} and 1.02 mm h^{-1}.

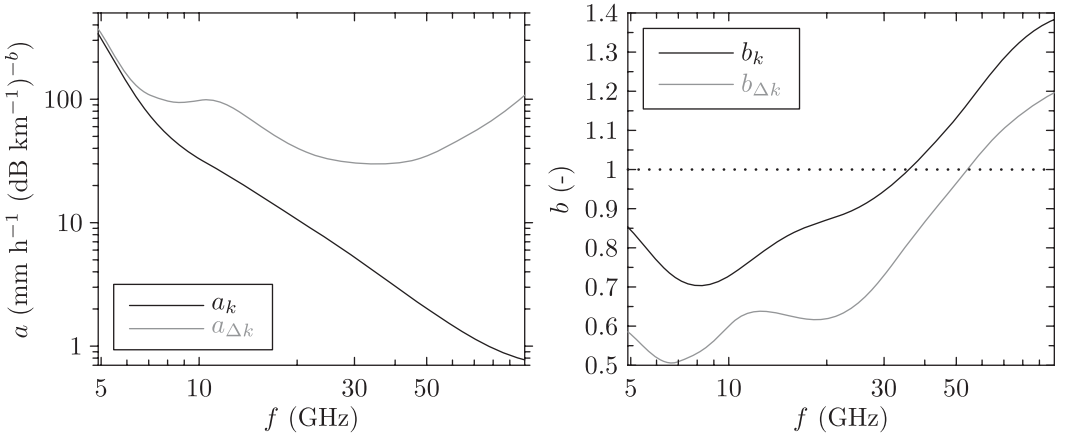

FIG. 2. (left) Coefficients and (right) exponents of R–k (black) and R–Δk (gray) power laws. In the right panel the $b = 1$ line (dotted line) indicates linearity.

c. Computation of link errors

Using measured drop size distributions [see section 2b] and $Q_{\text{ext}}(D)$ and $v(D)$ relations, values of k (dB km^{-1}) and R (mm h^{-1}) are computed (e.g., Atlas and Ulbrich 1977) according to

$$k = \frac{10^{-2}}{\ln(10)} \int_0^\infty Q_{\text{ext}}(D) N(D)\, dD, \quad \text{and} \tag{2}$$

$$R = 6 \times 10^{-4} \pi \int_0^\infty v(D) D^3 N(D)\, dD, \tag{3}$$

where $N(D)$ (mm^{-1} m^{-3}) is the number concentration of drops per unit diameter as a function of drop diameter. As in section 2, the $v(D)$ relation that is used here is that given by Beard (1976).

To retrieve rainfall intensities from specific attenuation, a retrieval relation is needed. Like many others (e.g., Hitschfeld and Bordan 1954; Wexler and Atlas 1963; Atlas and Ulbrich 1977; Olsen et al. 1978; Leijnse et al. 2007a,b), we will use power-law relations between R and k. In this paper, we will also consider differences in attenuation between horizontally and vertically polarized signals, as well as attenuation differences between signals at different frequencies. Among others, Holt et al. (2003) have suggested that these attenuation differences Δk are related to the rainfall intensity through power-law relations. Therefore, we will use such power-law relations for the retrieval of R from both k and Δk. In the remainder of this paper, k refers to the specific attenuation of a horizontally polarized signal.

Power-law relations between R on the one hand and k and Δk on the other have been derived using the De Bilt DSD dataset (see section 1). From these, (point scale) DSDs values of R, k, and Δk have been computed using Eqs. (2) and (3). Power laws have been fitted to these data using a nonlinear fit with a least squares criterion:

$$R = a_k k^{b_k}, \quad \text{and} \tag{4}$$

$$R = a_{\Delta k} (\Delta k)^{b_{\Delta k}}. \tag{5}$$

Figure 2 shows the coefficients and exponents of these power-law relations as functions of the signal frequency. Results are only shown for Δk computed from two signals with the same frequency and different polarizations (i.e., not with different frequencies). The power-law relations can be seen to be linear around 36 GHz for the R–k relation and around 54 GHz for the R–Δk relation. We expect that the errors and uncertainties will be limited around these frequencies because spatial variations will not cause large errors. Atlas and Ulbrich (1977) argued that the linearity of the R–k relation around 35 GHz stems from the fact that the terms $Q_{\text{ext}}(D)$ in Eq. (2) and $v(D)D^3$ in Eq. (3) have similar shapes. Besides linearity of the R–k relation, this also implies that this relation should be independent of the shape of $N(D)$.

From the left panel of Fig. 2 it is clear that, except for low frequencies, k is much more sensitive to R than Δk. This means that noise occurring in one of the signals needed for Δk may have a large effect on the accuracy. One of the largest advantages of using Δk is that other sources of signal variation (such as wet antenna attenuation, signal absorption by atmospheric constituents, transmitter/receiver drift, etc.) may be fully or partially cancelled out if these effects are independent of polarization for dual-polarization links (Ruf et al. 1996) or independent of frequency for dual-frequency links.

Dual-frequency link analyses will focus on frequency and polarization combinations found in the literature. Coefficients and exponents have been found for these

TABLE 1. *R–k* power-law coefficients and exponents for links employed in previous studies, of which frequency (f), polarization (Pol.; H for horizontal, V for vertical), and length (L) are given. If two polarizations or frequencies are indicated, Δk is used. If no information on the polarization is available in a given reference [Pol. = N/A in (e) and (h)–(m)], we have assumed the polarization to be horizontal. The letters in the first column will be used throughout the remainder of this paper to indicate the corresponding link settings.

	Source	Pol.	f (GHz)	L (km)	a_k, $a_{\Delta k}$	b_k, $b_{\Delta k}$
(a)	Ruf et al. (1996)	HV	35.0	0.51	30.0	0.80
(b)	Rincon and Lang (2002)	HH	25.4, 38.0	2.3	6.18	1.14
(c)	Holt et al. (2003) and Rahimi et al. (2003)	VV	12.8, 17.6	23.3	31.0	0.99
(d)	Rahimi et al. (2003, 2004) and Upton et al. (2005)	HH	13.9, 22.9	13.9	12.7	0.94
(e)	Minda and Nakamura (2005)	N/A	50.0	0.82	2.02	1.13
(f)	Krämer et al. (2005)	VV	10.5, 17.5	29.6	22.2	0.96
(g)	Upton et al. (2005)	H	22.9	13.9	8.4	0.89
(h)	Messer et al. (2006)	N/A	8.0	16.11	51.6	0.70
(i)	Messer et al. (2006)	N/A	18.0	5.8*	12.7	0.86
(j)	Messer et al. (2006)	N/A	18.0	9.48	12.7	0.86
(k)	Messer et al. (2006)	N/A	23.0	1.53	8.37	0.89
(l)	Leijnse et al. (2007b)	N/A	38.5	6.72	3.28	1.03
(m)	Leijnse et al. (2007a)	N/A	27.0	4.89	6.35	0.92

* There are three links with near-equal lengths (5.77, 5.86, and 5.88 km) in the same frequency band.

dual-frequency links as described above. Table 1 lists these coefficients and exponents, as well as link length, frequency, and polarization. These values are also given for some single-frequency links found in the literature. It should be noted that Rincon and Lang (2002) did not use Δk to retrieve $\overline{R}$, but they instead used both signals to derive two DSD parameters, from which the path-averaged rainfall intensity can then be computed.

The profiles of DSDs generated using the method described in section 3b are used to compute path-averaged specific attenuation ($\overline{k}$) and rainfall intensity $\overline{R}$ using Eqs. (2) and (3). The path-averaged specific attenuation is then used with Eq. (4) to retrieve the path-averaged rainfall intensity. The same procedure is followed for Δk measurements. These retrieved rainfall intensities are then compared to the true $\overline{R}$. Errors and uncertainties in link measurements are expressed by MBE and RMSE:

$$\mathrm{MBE} = \frac{1}{N_\mathrm{s}} \sum_{i=1}^{N_\mathrm{s}} (a\overline{k}_i^b - \overline{R}_i), \quad \text{and} \tag{6}$$

$$\mathrm{RMSE} = \sqrt{\frac{1}{N_\mathrm{s}} \sum_{i=1}^{N_\mathrm{s}} \left(a\overline{k}_i^b - \overline{R}_i - \mathrm{MBE}\right)^2}, \tag{7}$$

where N_s is the number of samples. Both of these quantities are normalized by the mean rainfall intensity to obtain a relative quantity. Unlike Berne and Uijlenhoet (2007), we have not used relative errors because the dataset used in this paper contains zero rainfall. In the remainder of this paper, the term errors will refer to MBE and uncertainties will refer to RMSE.

Leijnse et al. (2008) have presented these statistics based on the simulation of link signals from radar data (see section 2a). To be able to compare errors and uncertainties presented in this paper to those presented by Leijnse et al. (2008), these statistics are also computed with profiles of k or Δk that are computed from profiles of R using Eq. (4) or (5) (and not directly from the profiles of DSDs). The resulting statistics will be denoted by MBE_R and RMSE_R. In this sense, values of MBE and RMSE can be viewed as the combination of MBE_R and RMSE_R, respectively (i.e., errors and uncertainties caused purely by spatial variation in R), and the effect of the scatter of R and k pairs around the power-law *R–k* retrieval relation (see also section 5). It should be noted here that the computation of the profiles of k and Δk from profiles of R is performed using the same relations as those used for the retrieval of R from k or Δk (i.e., the power-law relations with coefficients and exponents presented in Fig. 2).

If we assume that the power-law relation between R and k is perfect (which we do for computing MBE_R), then MBE [see Eq. (6)] can be expressed as

$$\mathrm{MBE} = \frac{1}{N_\mathrm{s}} \sum_{i=1}^{N_\mathrm{s}} \left(a \left\{ \frac{1}{L} \int_0^L \left[\frac{R_i(s)}{a} \right]^{1/b} ds \right\}^b - \overline{R}_i \right), \quad \text{and} \tag{8}$$

$$\overline{R}_i = \frac{1}{L} \int_0^L R_i(s)\, ds. \tag{9}$$

Note that Eq. (8) is independent of a. Using the Taylor expansion of $R_i^{1/b}$ around $\overline{R}_i$, and truncating this series after the third term (i.e., assuming small deviations of R_i from $\overline{R}_i$) yields

$$\mathrm{MBE} = \frac{1}{N_s}\sum_{i=1}^{N_s}\left\{\overline{R}_i\left[1 + \frac{1}{2b}\left(\frac{1}{b} - 1\right)\mathrm{CV}_{R,i}^2\right]^b - \overline{R}_i\right\}, \tag{10}$$

where $\mathrm{CV}_{R,i}$ is the coefficient of variation of R_i over the link. It can easily be seen from this expression that MBE should be positive when $0 < b < 1$ and negative when $b > 1$. Hence, the expected behavior of MBE is that, if the influence of DSD variations is limited around frequencies where b is close to 1, there should be a sign change. Given the dependency of b on the signal frequency (see Fig. 2), MBE is expected to be positive at low frequencies and negative at high frequencies.

4. Validity of Taylor's hypothesis

Because the radar (see section 2a) does not provide information on the size distribution of raindrops, we can only examine the validity of Taylor's hypothesis in terms of the rainfall intensity $R(x, t)$, where x is the distance from the radar, and t is time. Note that the selected radial in the radar dataset (Leijnse et al. 2008) is the predominant wind direction for the region under consideration. Hence, the test performed here is not only a test of Taylor's hypothesis but also of whether subsequent analyses will yield results that are valid for a link with fixed orientation (in the predominant wind direction). Rainfall advection velocities are estimated from the radar data. It is assumed that this advection velocity is constant in space and time for the entire event. For each separate event, the effective parallel advection velocity u is determined by fitting $R(x_0 + \Delta x, t_0 + \Delta x/u)$ to $R(x_0, t_0)$. This fit is accomplished by finding the value of u that minimizes the sum of squared errors

$$\mathrm{SSE}(u) = \sum_{i=-N_x}^{N_x}\sum_{j=1}^{N_t}\left[R(x_i, t_j) - R\left(x_0, t_j + \frac{x_i - x_0}{u}\right)\right]^2 \tag{11}$$

in the range $-50\ \mathrm{m\ s^{-1}} < u < 50\ \mathrm{m\ s^{-1}}$ (corresponding to the maximum advection velocities found by de Lannoy et al. 2005, in the same climate). In Eq. (11), x_0 is the location of the midpoint of the link, N_t is the number of time intervals in the event, and N_x is the number of samples in the range direction (on either side of x_0) that are considered. For these analyses, $N_x = 8$, corresponding to a maximum Δx of approximately ± 2 km. This distance has been chosen to obtain robust estimates of the advection velocity u while retaining the local character of typical wind measurements. In Eq. (11), the value of $R[x_0, t_j + (x_i - x_0)/u]$ is determined by linearly interpolating $R(x_0, t)$ between the nearest available time intervals.

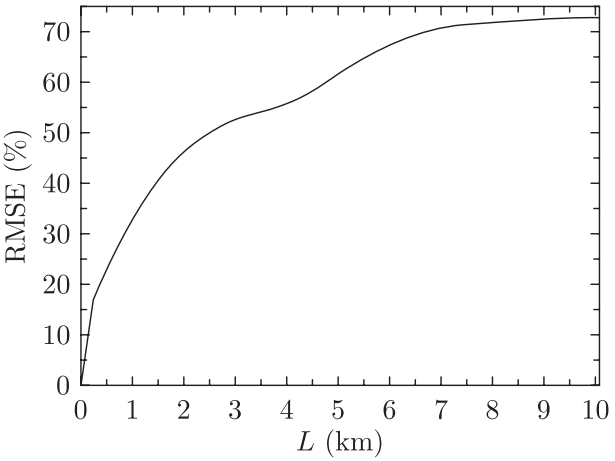

FIG. 3. RMSE (%) between the true path-averaged rainfall intensity and that derived using Taylor's hypothesis as a function of the pathlength L.

To examine the validity of Taylor's hypothesis, the root-mean-square error of path-averaged rainfall intensities determined using Taylor's hypothesis is computed. This RMSE is computed over all 332 rainfall events. Figure 3 shows the RMSE, normalized with the mean rainfall intensity, as a function of length of the path over which the rainfall is averaged (which corresponds to the link length L in the remainder of this paper). This figure shows that the normalized RMSE increases quite rapidly with the pathlength (or link length) L. However, the RMSE is very sensitive to large values, which are well known to be highly local in both space and time for rainfall (e.g., Berne et al. 2004b; Ciach and Krajewski 2006). Furthermore, the link error statistics derived from these data only depend on the distribution of R along the link, whereas the RMSE presented in Fig. 3 depends on the direct comparison of $R(x, t)$ to $R(x + \Delta x, t + \Delta x/u)$. Even though this latter comparison may quickly become worse with increasing Δx, the distribution of R along a link can still be similar. Therefore, we also investigate the effect of using Taylor's hypothesis on these derived link error statistics, which is ultimately what is of relevance here. These statistics can then be compared to those not based on Taylor's hypothesis (Leijnse et al. 2008).

Figure 4 shows comparisons of normalized MBE [see Eq. (6)], and normalized RMSE [see Eq. (7)] as functions of link length and signal frequency. It can be concluded from this figure that the link error statistics are very similar, and that Taylor's hypothesis can be used for this purpose under the given climatic conditions and assuming that the spatial structure of drop size distributions follows that of the rainfall intensity.

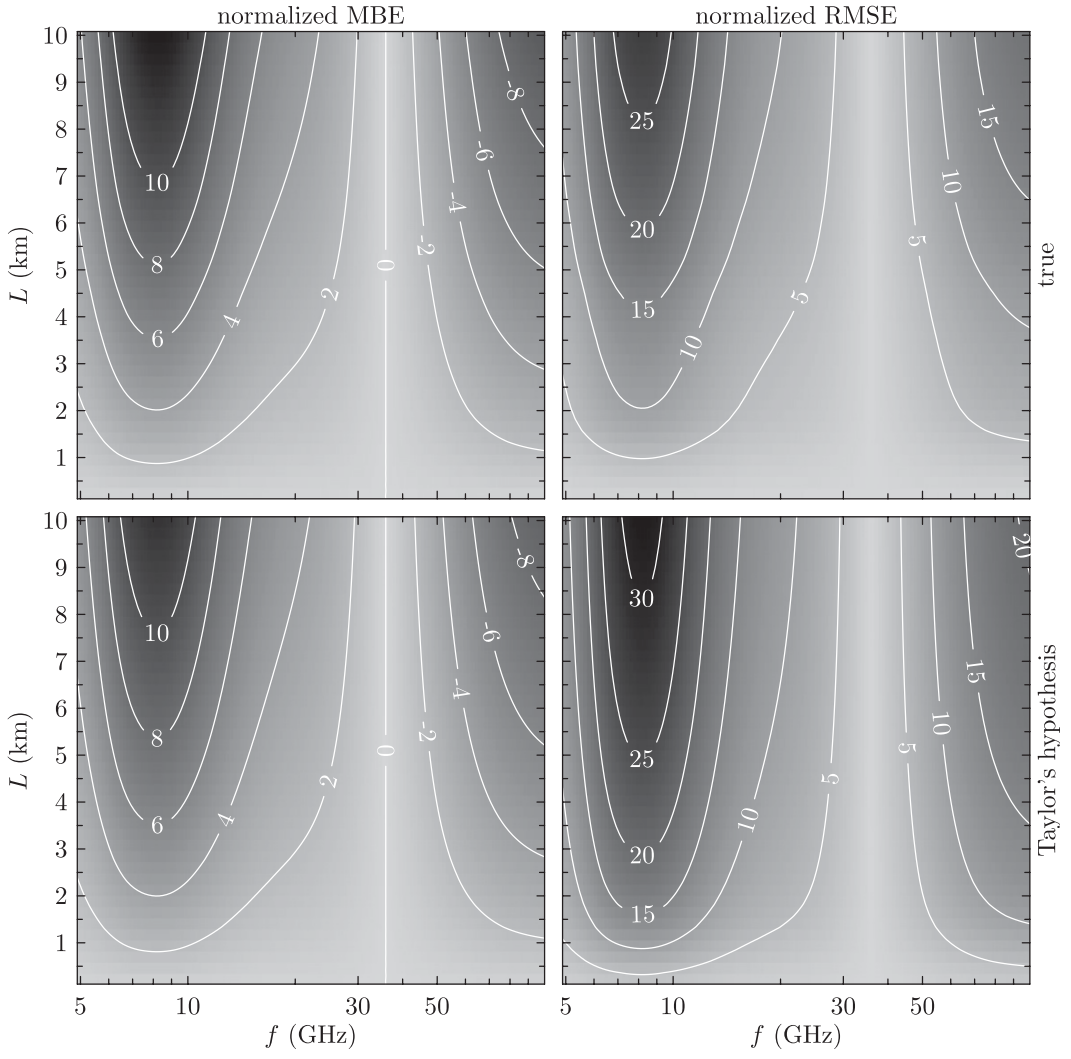

FIG. 4. (left) Normalized MBE (%) and (right) normalized bias-corrected RMSE (%) in R as functions of link frequency (x axis) and length (y axis). (top) Results when all range cells of the radar dataset are used, and (bottom) results when Taylor's hypothesis is used in combination with the time series of only the center pixel of the radar dataset are shown.

Advection velocities of rainstorms can be different from low-level wind velocities. To investigate this, we compare wind velocities measured at 10 m at the nearby (6.5 km to the southwest of the radar) Rotterdam Airport meteorological station to rainfall advection velocities derived from the radar. The correlation between the radar-estimated rainstorm advection velocities in the direction of the selected radial and the event average of the corresponding component of the 10-m wind vector is 0.56. Based on this, we assume that low-level wind velocities can be used as a proxy for rainstorm advection velocities for this application. Because the magnitude of low-level wind velocities is usually smaller than that of advection velocities, we compare statistics of wind velocities measured at 200 m at the CESAR site during rain to statistics of the advection velocities u discussed above. The mean 200-m wind velocity during rain is 8.7 m s^{-1} (coefficient of variation CV = 0.43), while the mean absolute advection velocity derived in testing Taylor's hypothesis is 20.9 m s^{-1} (CV = 0.52). We therefore apply a correction factor of 2.4 (the ratio of these means) to the measured 200-m wind velocities to arrive at approximate rainstorm advection velocities.

5. Errors and uncertainties related to variations in DSDs

Errors and uncertainties in retrieved rainfall intensities from microwave link measurements due to rainfall variability can be attributed to two factors. The first is

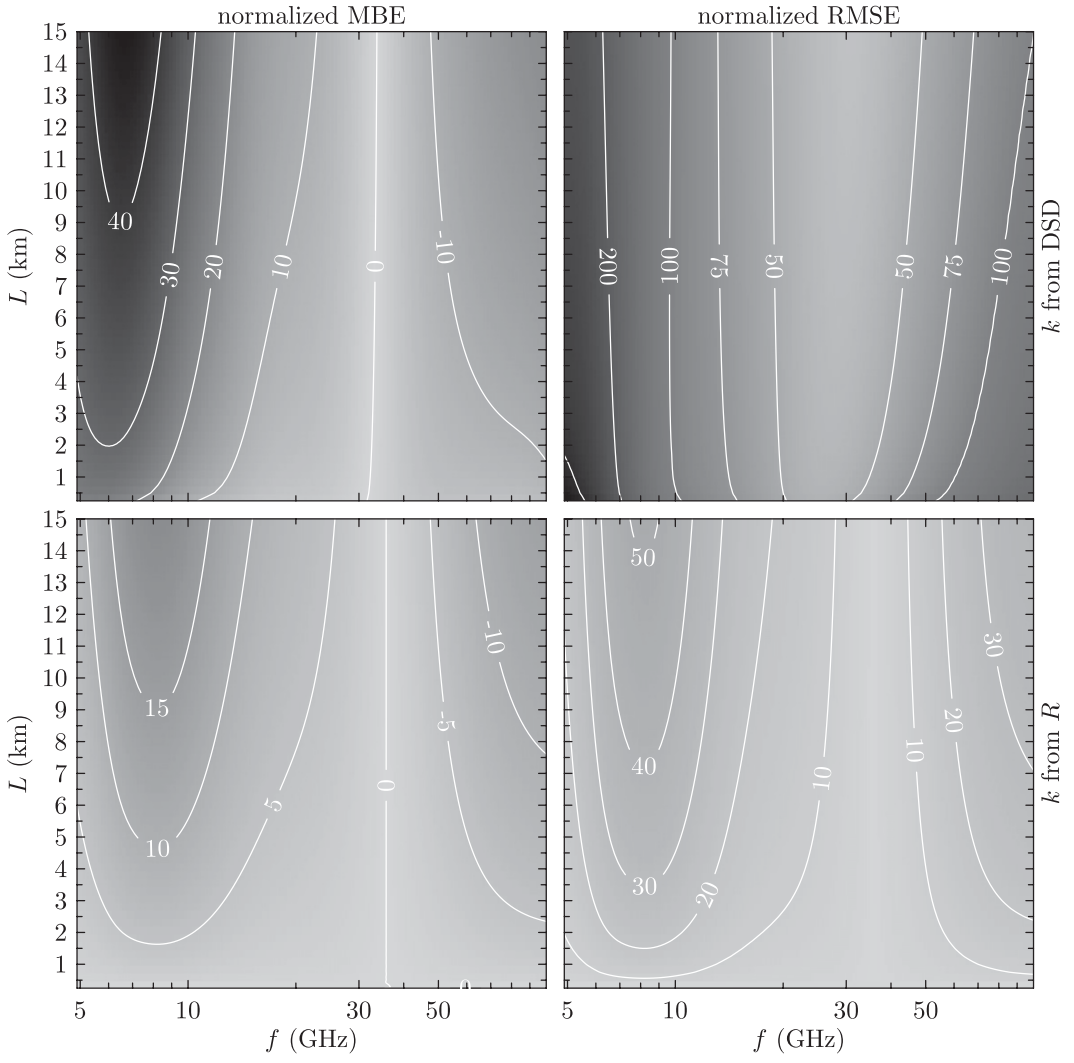

FIG. 5. (left) Normalized MBE (%) and (right) RMSE (%) in the retrieved rainfall intensity as functions of link frequency (x axis) and length (y axis) for horizontally polarized signals. Gray scale is logarithmic above RMSE = 100% in the right panel. (top) Profiles of k that have been derived from DSDs directly are shown. (bottom) Profiles of k that have been derived from profiles of R using the R–k relations from Fig. 2 are shown.

the interplay between the variation of the rainfall intensity along the link path and the nonlinearity of the R–k retrieval relation. The second is the variation of the shape of the DSD, which may cause the employed R–k relation to be suboptimal for the given path-averaged DSD at a given moment. As noted in section 3, it is expected that both of these factors will be at a minimum at link frequencies where the R–k relation is close to linear.

Results of simulations of errors and uncertainties (MBE and RMSE, respectively) from profiles of DSDs for horizontally polarized link signals are shown in Fig. 5. The bottom panels of this figure show these statistics when the attenuation is determined from R, and not directly from DSDs, as is shown in the top panels. To check the consistency between the analyses presented in section 4 (testing Taylor's hypothesis), we first compare the bottom panels of Fig. 5 to the bottom panels of Fig. 4. These figures should be similar because they show essentially the same statistics for the same climate (albeit determined over a different time period and using a different instrument). In comparing these figures, it should be noted that the L axes of these figures are different (maximum L of 10.08 km in Fig. 4 and 15 km in the bottom panels of Fig. 5). Both MBE and RMSE can be seen to be somewhat higher in the bottom panels of Fig. 5, but the general shape is similar. These differences can be explained by the different nature of the two instruments used. In particular, the differences in sampling volume will cause the profiles of R generated using the 2DVD to be more variable, resulting in larger errors. The true

rainfall variability experienced by a link will be somewhere in between, as the sampling volume of a link is larger than that of a disdrometer and smaller than that of a radar. However, we judge these graphs to be sufficiently similar for both the analyses presented in Leijnse et al. (2008) and those presented in this paper to be useful.

The results presented in Fig. 5 show that the least severe errors and uncertainties occur at frequencies around 30 GHz. This is to be expected as the R–k power-law relation is close to linear at this frequency. As mentioned before, this linearity is caused by the similarity of the terms $Q_{\text{ext}}(D)$ in Eq. (2) and $v(D)D^3$ in Eq. (3). As a consequence of this similarity, the dependence on the shape of $N(D)$ is small (although it still plays a role). At other frequencies, the severity of the bias (absolute value of MBE) is seen to monotonically increase with link length, which is a consequence of increased rainfall variation along the link in combination with a nonlinear R–k retrieval relation. Comparison with the bottom left panel of Fig. 5 shows that the scatter around the R–k relation caused by DSD variability plays a large role in this, as the MBE purely caused by spatial variation in R is much smaller.

The errors and especially the uncertainties shown in the top panels of Fig. 5 are at a minimum at a frequency that is lower than the frequency at which the minima in the bottom panels of Fig. 5 occur. This is due to the fact that the maximum DSD-weighted degree of similarity between the terms $Q_{\text{ext}}(D)$ in Eq. (2) and $v(D)D^3$ in Eq. (3) does not occur at the same frequency as that where the optimal R–k relation is linear. This shows that the influence of the shape of $N(D)$ does play a role at these frequencies. Unlike in the bottom-right panel of Fig. 5, the RMSE is seen to monotonically decrease with link length. The reason for this is that the scatter around the R–k relation caused by DSD variability along the link will decrease because of averaging. This masks the effect of the increase of variability of R along a link, which can be seen to be much smaller in the bottom panels of Fig. 5.

It can be stated that for single-frequency single-polarization links, the errors and uncertainties related to spatial DSD variability are limited (i.e., $|\text{MBE}| < 10\%$ and $\text{RMSE} < 50\%$) for link frequencies between 20 and 40 GHz and link lengths between 2 and 10 km. For other frequencies, these statistics are worse, especially at low frequencies, where the MBE is still acceptable for short links; however, the RMSE is very large regardless of the link length.

Simulation results using Δk from differently polarized signals are shown in Fig. 6. In terms of MBE, the frequency at which errors are least severe is close to that where the R–Δk relation is close to linear (i.e., around 55 GHz). Comparison of the top and bottom left-hand panels of Fig. 6 reveals that above approximately 40 GHz the effect of DSD shape variability on the bias (MBE) is small compared to the effect of variability of R. Below this frequency, this effect rapidly increases with decreasing frequency. As expected, the MBE increases monotonically with link length, which was also seen for $\overline{R}$ retrieved from $\overline{k}$, especially at lower frequencies, where the shape of the top and bottom left-hand panels of Fig. 6 is different. This indicates that spatial averaging of R and Δk causes a bias with respect to the employed R–Δk relation that has a different frequency dependence than the combined influence of nonlinearity of the R–Δk relation and R variability, which means that the shape of the DSD plays a large role in the MBE at low frequencies.

At frequencies above approximately 40 GHz, the RMSE is small compared to other frequency regions and decreases with link length. At lower frequencies (below ~30 GHz), the effects of the combination of the nonlinearity of the R–Δk relation and the variability in R become apparent in the top-right panel of Fig. 6, as the RMSE no longer decreases monotonically with link length, and the values of RMSE in the bottom-right panel of Fig. 6 are of similar orders of magnitude (albeit smaller). In the frequency range between 40 and 80 GHz and for links longer than 2 km $|\text{MBE}| < 5\%$ and $\text{RMSE} < 50\%$.

Figure 7 shows errors and uncertainties in $\overline{R}$ retrieved from $\overline{\Delta k}$ for dual-frequency links with frequency and polarization combinations encountered in the literature [links (b), (c), (d), and (f) in Table 1]. The difference in errors between link (b) (Rincon and Lang 2002) and the other dual-frequency links found in the literature is striking, especially regarding the RMSE. The fact that a link with these settings performs much worse than the others can be explained by the fact that the exponents of the power-law retrieval relations for this link deviate much more from 1 than the others (see Table 1). As stated before, the degree of deviation from 1 of the power-law exponent is not only a measure of the nonlinearity of the relation (and hence the sensitivity to spatial variability) but also a measure of the sensitivity to DSD shape variability (Atlas and Ulbrich 1977). The bottom panels of Fig. 7 show that the effect of the combination of nonlinear R–Δk relations and the spatial variability of R is indeed greatest for link (b) (both in terms of MBE and RMSE), but that the order of magnitude of the effect of scatter around the R–Δk relation due to DSD shape variability is much greater. As stated in section 3, it should be noted here that Rincon and Lang (2002) did not retrieve $\overline{R}$ from $\overline{\Delta k}$. Hence, the large

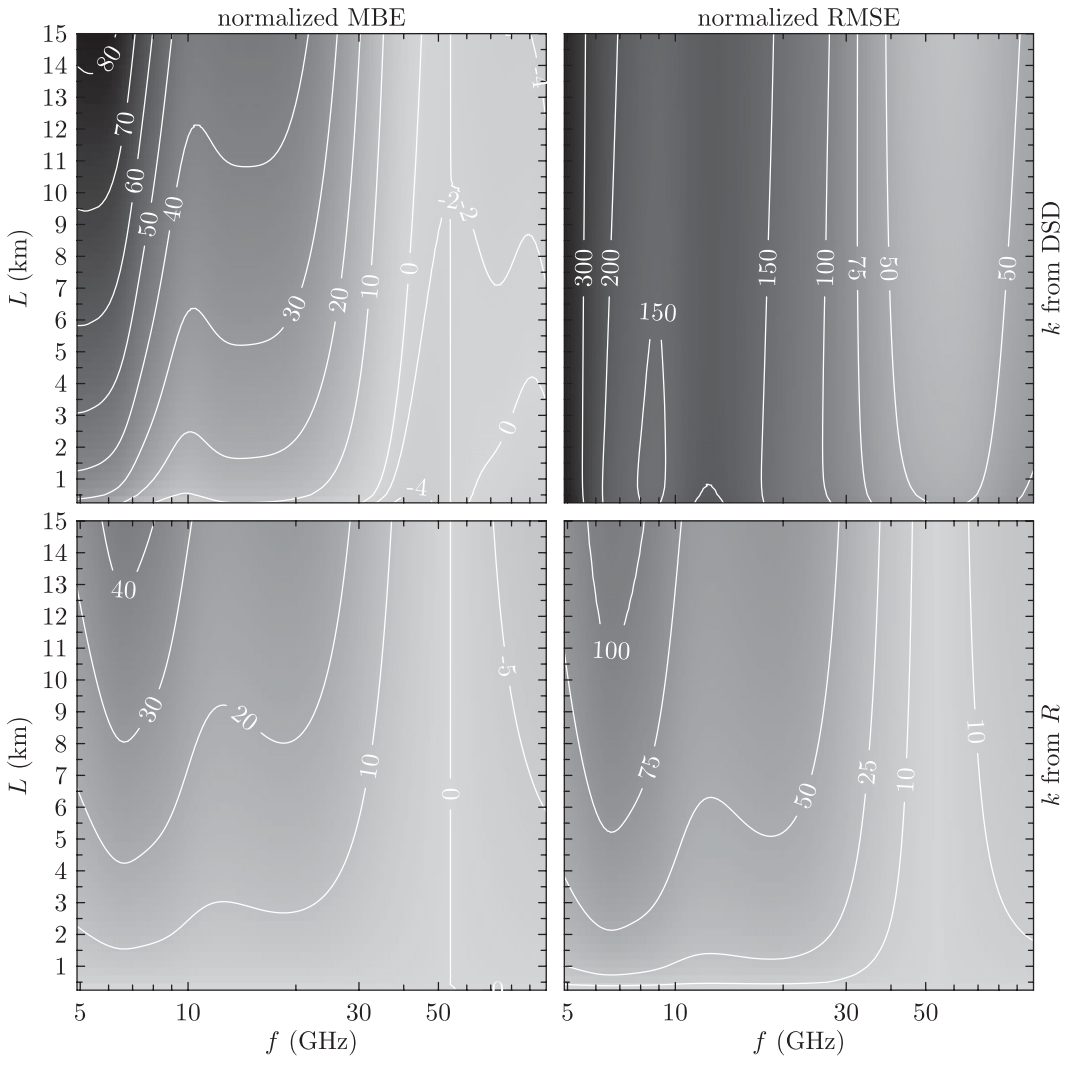

FIG. 6. (left) Normalized MBE (%) and (right) RMSE (%) in the rainfall intensity retrieved from Δk from orthogonally polarized signals as functions of link frequency (x axis) and length (y axis). Gray scale is logarithmic above RMSE = 100% in the right panel. (top) Profiles of k that have been derived from DSDs directly are shown. (bottom) Profiles of k that have been derived from profiles of R using the R–k relations from Fig. 2 are shown.

values of |MBE| and RMSE found here do not apply to their study.

The other dual-frequency link settings [(c), (d), and (f)] perform equally well or better than single-frequency links (see Fig. 5), with similar dependencies on link length. It is interesting to note (see Fig. 7) that for the low-frequency links [(c) and (f)], the bias with respect to the R–Δk relations introduced by DSD shape variability acts to compensate the effect of the combination of the nonlinear R–Δk relations and the spatial variability of R in the MBE.

Table 2 lists the errors and uncertainties in retrieved $\overline{R}$ for links found in the literature (see Table 1 for link characteristics). This table essentially lists values that can be found in Figs. 5–7. Figure 8 shows the MBE and RMSE from Table 2 as functions of the corresponding power-law exponents b from Table 1. Also shown in this figure are the MBE and RMSE from the top panels of Figs. 5 and 6 for all link lengths (i.e., between 0.25 and 15 km) and frequencies (i.e., between 5 and 100 GHz) considered. It should be noted that, because we have restricted the normalized RMSE to values below 150% in Fig. 8, the data from Fig. 5 are only shown for frequencies above 7.5 GHz, and the data from Fig. 6 are only shown for frequencies higher than 18 GHz. The seemingly abrupt ends to and folding of the surfaces in Fig. 8 are caused by the fact that only frequencies between 5 and 100 GHz have been considered, and the fact that the relation between b and f is not monotonic (see Fig. 2).

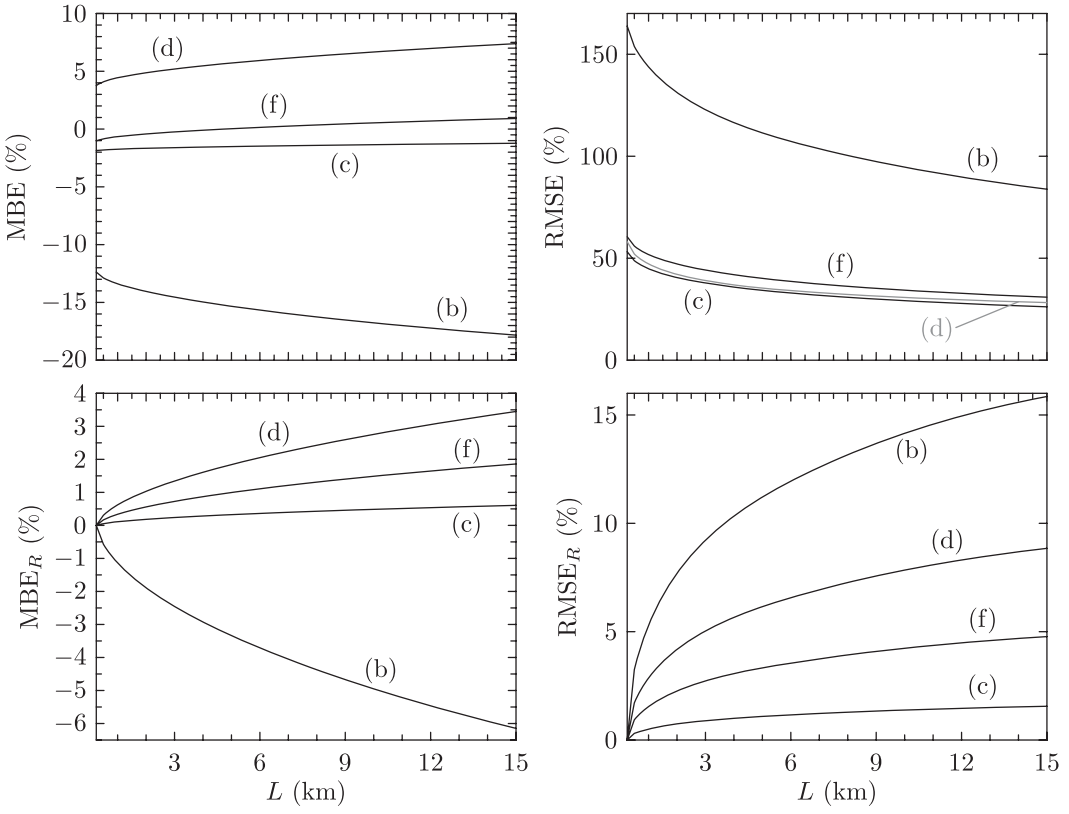

FIG. 7. (left) Normalized MBE (%) and (right) RMSE (%) in the rainfall intensity retrieved from Δk from signals with different frequencies as functions of link length for frequency and polarization combinations found in the literature [see Table 1 for references corresponding to (b),(c),(d), and (f)]. For clarity, the line corresponding to link (d) is gray in the right panel. (top) Profiles of k that have been derived from DSDs directly are shown. (bottom) Profiles of k that have been derived from profiles of R using the R–k relations from Fig. 2 are shown.

The fact that the normalized MBE is nonzero for $b = 1$ indicates that the employed R–k relation is not unbiased at the point scale. What is most striking about Fig. 8 is the fact that the value of b is able to explain a large part of the variation in both MBE and RMSE. Especially that the RMSE shows a very clear dependence on b, regardless of the lengths of the links. The importance of the proximity of b to 1 for both MBE and RMSE again shows that b not only determines the linearity of the relation but also the degree of dependence on DSD shape. The dependence of the values of MBE on b is not as clear as for the RMSE, as was to be expected as the dependence on link length is greater for MBE than it is for RMSE (see Figs. 5 and 7). However, the exponent of the point-scale relation b could still be used to obtain a first estimate of MBE and RMSE that is to be expected for a given link frequency or combination of frequencies.

6. Conclusions

The main objective of this paper was to assess the errors and uncertainties in microwave link estimates of path-averaged rainfall intensities caused by rainfall variability. A nearly 2-yr-long dataset of drop size distributions has been used in combination with wind measurements made at 200 m to simulate link signals to compute these statistics. To assess the validity of the results from these analyses, Taylor's hypothesis has been tested using more than 1.5 yr of high-resolution radar data. It is shown that in terms of squared differences between path-averaged rainfall intensities computed from spatiotemporal data and those computed from temporal data using Taylor's hypothesis, the validity of this hypothesis quickly decreases with distance. However, the hypothesis can still safely be used for the analyses presented in this paper, as the error statistics produced using Taylor's hypothesis are very similar to those not based on this hypothesis.

Arrival times, drop sizes, and velocities measured by a 2DVD at CESAR (the Netherlands) over a period spanning nearly 2 yr have been used in combination with wind velocity measurements to generate range profiles of DSDs. These profiles have been used to compute corresponding profiles of rainfall intensities and specific

TABLE 2. Normalized MBE (%) and RMSE (%) in retrieved rainfall intensity for links employed in previous studies, with profiles of k generated from profiles of DSDs as well as profiles of R (denoted by the subscript R). For the meaning of the letters in the first column and the corresponding link characteristics, see Table 1. For links with lengths longer than 15 km [i.e., (c), (f), and (h)], results have been linearly extrapolated.

Source	MBE	RMSE	MBE_R	$RMSE_R$
(a)	−1.56	73.06	1.04	5.71
(b)	−14.21	128.39	−2.07	8.22
(c)	−1.04	22.09	0.79	1.78
(d)	7.24	28.70	3.31	8.67
(e)	−6.19	84.74	−0.93	4.48
(f)	1.92	22.83	2.84	5.98
(g)	9.72	36.57	5.94	15.53
(h)	42.91	131.94	20.93	52.26
(i)	9.26	53.95	4.70	15.12
(j)	10.94	53.10	6.26	18.00
(k)	5.03	39.72	1.52	6.45
(l)	−3.97	41.63	−0.83	2.61
(m)	4.56	31.78	2.31	7.75

attenuations (at different frequencies and polarizations). Using these profiles, the effect of the variation in DSDs along a simulated microwave link has been studied as a function of its length and frequency. For these analyses, retrieval relations have been used that are based on a different drop size dataset to guarantee independence.

For single-frequency single-polarization links, the errors and uncertainties (i.e., normalized MBE and RMSE, respectively) related to spatial DSD variability are limited (|MBE| <10% and RMSE <50%) for links with frequencies between 20 and 40 GHz and lengths between 2 and 10 km. When using the difference in attenuation between horizontally and vertically polarized signals this range is between 40 and 80 GHz with $L >$ 2 km. For frequencies outside these ranges, these statistics are worse. Especially at low frequencies, the MBE is still acceptable for short links, but the RMSE is very large regardless of the link length.

For all types of link data (specific attenuation, attenuation difference between signals with orthogonal polarizations, or different frequencies) errors in the retrieved path-averaged rainfall intensities (|MBE|) generally increase with link length and uncertainties (RMSE) generally decrease with link length. Both of these statistics are at a minimum near the frequency at which the retrieval relation is linear. This is due to the fact that the phenomenon that causes the retrieval relation to be linear also causes the results to be relatively insensitive to the shape of the DSD at these frequencies. This is also the reason why there is little dependence on the length of the link at these frequencies.

We have shown that the exponent of the point-scale power-law R–k or R–Δk relation can explain a large part of the variation in both MBE and RMSE. This means that the order of magnitude of these error statistics can be predicted from the value of this exponent, regardless of the link length. The fact that the link length only has a second-order effect on bias and especially uncertainty indicates that the point-scale retrieval relation and the scatter around it play a very important role in microwave link rainfall estimation.

Acknowledgments. The authors thank Michael Schönhuber and Günter Lammer of Joanneum Research for their help with the 2DVD instrument, Bertram Arbesser-Rastburg of ESA-ESTEC for the use of the 2DVD, and Herman Russchenberg and Fred van der

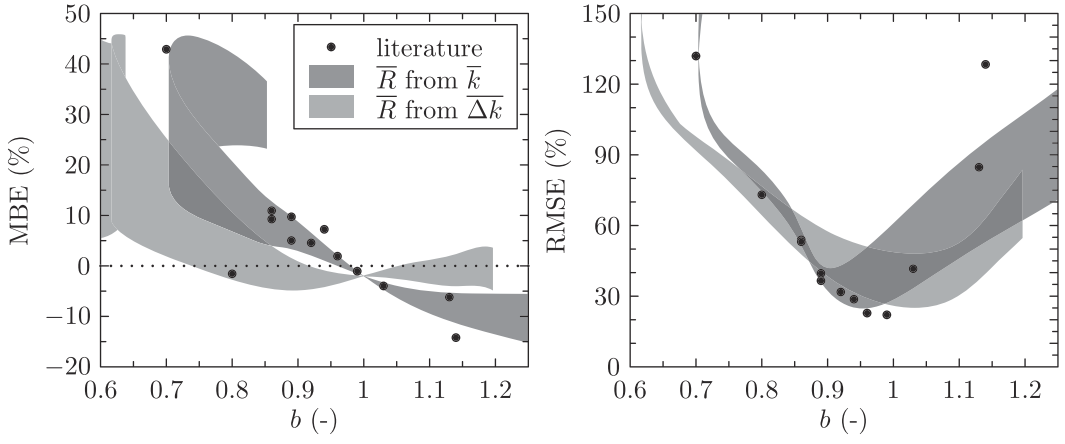

FIG. 8. (left) Normalized MBE (%) and (right) RMSE (%) as functions of the power-law exponent b of the retrieval relation for link configurations found in the literature (see Tables 1 and 2) and for the analyses presented in this paper (see Fig. 5 for $\overline{R}$ from $\overline{k}$ and Fig. 6 for $\overline{R}$ from $\overline{\Delta k}$). Shaded areas indicate the spread in MBE and RMSE for links with lengths between 0.25 and 15 km.

Zwan of TU Delft for the radar data and their help in interpreting them. All wind data used in this paper (from the Rotterdam Airport meteorological station and from the CESAR site) were collected by the Royal Netherlands Meteorological Institute. H. Leijnse was financially supported by the Netherlands Organisation for Scientific Research (NWO) through a grant in the framework of the Water Programme.

REFERENCES

Andsager, K., K. V. Beard, and N. F. Laird, 1999: Laboratory measurements of axis ratios for large raindrops. *J. Atmos. Sci.,* **56,** 2673–2683.

Atlas, D., and C. W. Ulbrich, 1977: Path- and area-integrated rainfall measurement by microwave attenuation in the 1–3-cm band. *J. Appl. Meteor.,* **16,** 1322–1331.

Aydin, K., and S. E. A. Daisley, 2002: Relationships between rainfall rate and 35-GHz attenuation and differential attenuation: Modeling the effects of raindrop size distribution, canting, and oscillation. *IEEE Trans. Geosci. Remote Sens.,* **40,** 2343–2352.

Beard, K. V., 1976: Terminal velocity and shape of cloud and precipitation drops aloft. *J. Atmos. Sci.,* **33,** 851–864.

Berne, A., and R. Uijlenhoet, 2005: A stochastic model of range profiles of raindrop size distributions: Application to radar attenuation correction. *Geophys. Res. Lett.,* **32,** L10803, doi:10.1029/2004GL021899.

——, and ——, 2007: Path-averaged rainfall estimation using microwave links: Uncertainty due to spatial rainfall variability. *Geophys. Res. Lett.,* **34,** L07403, doi:10.1029/2007GL029409.

——, G. Delrieu, H. Andrieu, and J.-D. Creutin, 2004a: Influence of the vertical profile of reflectivity on radar-estimated rain rates at short time steps. *J. Hydrometeor.,* **5,** 296–310.

——, ——, J.-D. Creutin, and C. Obled, 2004b: Temporal and spatial resolution of rainfall measurements required for urban hydrology. *J. Hydrol.,* **299,** 166–179.

Ciach, G. J., and W. F. Krajewski, 2006: Analysis and modelling of spatial correlation structure in small-scale rainfall in Central Oklahoma. *Adv. Water Resour.,* **29,** 1450–1463.

Czekala, H., S. Havemann, K. Schmidt, T. Rother, and C. Simmer, 1999: Comparison of microwave radiative transfer calculations obtained with three different approximations of hydrometeor shape. *J. Quant. Spectrosc. Radiat. Transfer,* **63,** 545–558.

de Lannoy, G. J. M., N. E. C. Verhoest, and F. P. de Troch, 2005: Characteristics of rainstorms over a temperate region derived from multiple time series of weather radar images. *J. Hydrol.,* **307,** 126–144.

Grum, M., S. Krämer, H.-R. Verworn, and A. Redder, 2005: Combined use of point rain gauges, radar, microwave link, and level measurements in urban hydrological modelling. *Atmos. Res.,* **77,** 313–321.

Hitschfeld, W., and J. Bordan, 1954: Errors inherent in the radar measurement of rainfall at attenuating wavelengths. *J. Meteor.,* **11,** 58–67.

Holt, A. R., G. G. Kuznetsov, and A. R. Rahimi, 2003: Comparison of the use of dual-frequency and single-frequency attenuation for the measurement of rainfall along a microwave link. *IEE Proc. Microwaves Antennas Propag.,* **15,** 315–320.

Krämer, S., H.-R. Verworn, and A. Redder, 2005: Improvement of X-band radar rainfall estimates using a microwave link. *Atmos. Res.,* **77,** 278–299.

Kruger, A., and W. F. Krajewski, 2002: Two-dimensional video disdrometer: A description. *J. Atmos. Oceanic Technol.,* **19,** 602–617.

Leijnse, H., cited 2007: Hydrometeorological application of microwave links: Measurement of evaporation and precipitation. Ph.D. thesis, Wageningen University, 134 pp. [Available online at http://library.wur.nl/wda/dissertations/dis4353.pdf.]

——, R. Uijlenhoet, and J. N. M. Stricker, 2007a: Hydrometeorological application of a microwave link: 2. Precipitation. *Water Resour. Res.,* **43,** W04417, doi:10.1029/2006WR004989.

——, ——, and ——, 2007b: Rainfall measurement using radio links from cellular communication networks. *Water Resour. Res.,* **43,** W03201, doi:10.1029/2006WR005631.

——, ——, and ——, 2008: Microwave link rainfall estimation: Effects of link length and frequency, temporal sampling, power resolution, and wet antenna attenuation. *Adv. Water Resour.,* **31,** 1481–1493.

——, and Coauthors, 2010: Precipitation measurement at CESAR, the Netherlands. *J. Hydrometeor.,* **11,** 1332–1339.

Liebe, H. J., G. A. Hufford, and T. Manabe, 1991: A model for the complex permittivity of water at frequencies below 1 THz. *Int. J. Infrared Millimeter Waves,* **12,** 659–675.

Ligthart, L. P., and L. R. Nieuwkerk, 1990: An X-band solid-state FM-CW weather radar. *IEE Proc. F Radar Signal Processes,* **137,** 418–426.

Marshall, J. S., and W. M. Palmer, 1948: The distribution of raindrops with size. *J. Meteor.,* **5,** 165–166.

Messer, H. A., A. Zinevich, and P. Alpert, 2006: Environmental monitoring by wireless communication networks. *Science,* **312,** 713.

Minda, H., and K. Nakamura, 2005: High temporal resolution path-average raingauge with 50-GHz band microwave. *J. Atmos. Oceanic Technol.,* **22,** 165–179.

Mishchenko, M. I., 2000: Calculation of the amplitude matrix for a nonspherical particle in a fixed orientation. *Appl. Opt.,* **39,** 1026–1031.

——, L. D. Travis, and D. W. Mackowski, 1996: *T*-matrix computations of light scattering by nonspherical particles: a review. *J. Quant. Spectrosc. Radiat. Transfer,* **55,** 535–575.

Olsen, R. L., D. V. Rogers, and D. B. Hodge, 1978: The aR^b relation in the calculation of rain attenuation. *IEEE Trans. Antennas Propag.,* **26,** 318–329.

Overeem, A., A. Buishand, and I. Holleman, 2008: Rainfall depth–duration–frequency curves and their uncertainties. *J. Hydrol.,* **348,** 124–134.

——, ——, and ——, 2009a: Extreme rainfall analysis and estimation of depth–duration–frequency curves using weather radar. *Water Resour. Res.,* **45,** W10424, doi:10.1029/2009WR007869.

——, I. Holleman, and A. Buishand, 2009b: Derivation of a 10-year radar-based climatology of rainfall. *J. Appl. Meteor. Climatol.,* **48,** 1448–1463.

Rahimi, A. R., A. R. Holt, G. J. G. Upton, and R. J. Cummings, 2003: The use of dual-frequency microwave links for measuring path-averaged rainfall. *J. Geophys. Res.,* **108,** 4467, doi:10.1029/2002JD003202.

——, G. J. G. Upton, and A. R. Holt, 2004: Dual-frequency links—A complement to gauges and radar for the measurement of rain. *J. Hydrol.,* **288,** 3–12.

Rincon, R. F., and R. H. Lang, 2002: Microwave link dual-wavelength measurements of path-average attenuation for the estimation of drop size distributions and rainfall. *IEEE Trans. Geosci. Remote Sens.,* **40,** 760–770.

Ruf, C. S., K. Aydin, S. Mathur, and J. P. Bobak, 1996: 35-GHz dual-polarization propagation link for rain-rate estimation. *J. Atmos. Oceanic Technol.,* **13,** 419–425.

Schönhuber, M., H. Urban, J. P. V. Poiares Baptista, W. L. Randeu, and W. Riedler, 1994: Measurements of precipitation characteristics by a new disdrometer. *Proc. Atmospheric Physics and Dynamics in the Analysis and Prognosis of Precipitation Fields,* Rome, Italy.

Schuurmans, J. M., M. F. P. Bierkens, E. J. Pebesma, and R. Uijlenhoet, 2007: Automatic prediction of high-resolution daily rainfall fields for multiple extents: The potential of operational radar. *J. Hydrometeor.,* **8,** 1204–1224.

Sheppard, B. E., and P. I. Joe, 2000: Automated precipitation detection and typing in winter: A two-year study. *J. Atmos. Oceanic Technol.,* **17,** 1493–1507.

Thurai, M., and V. N. Bringi, 2005: Drop axis ratios from a 2D Video Disdrometer. *J. Atmos. Oceanic Technol.,* **22,** 966–978.

Tokay, A., P. G. Bashor, and K. R. Wolff, 2005: Error characteristics of rainfall measurements by collocated Joss-Waldvogel disdrometers. *J. Atmos. Oceanic Technol.,* **22,** 513–527.

Uijlenhoet, R., 1999: Parameterization of rainfall microstructure for radar meteorology and hydrology. Ph.D. thesis, Wageningen University, 279 pp.

——, J. M. Porrà, D. Sempere Torres, and J.-D. Creutin, 2006: Analytical solutions to sampling effects in drop size distribution measurements during stationary rainfall: Estimation of bulk rainfall variables. *J. Hydrol.,* **328,** 65–82.

Upton, G. J. G., A. R. Holt, R. J. Cummings, A. R. Rahimi, and J. W. F. Goddard, 2005: Microwave links: The future for urban rainfall measurement? *Atmos. Res.,* **77,** 300–312.

van de Beek, C. Z., H. Leijnse, J. N. M. Stricker, R. Uijlenhoet, and H. W. J. Russchenberg, 2010a: Performance of high-resolution X-band radar for rainfall measurement in the Netherlands. *Hydrol. Earth Syst. Sci.,* **14,** 205–221.

——, ——, P. J. J. F. Torfs, and R. Uijlenhoet, 2010b: Climatology of daily rainfall semivariance in the Netherlands. *Hydrol. Earth Syst. Sci. Discuss.,* **7,** 2085–2120.

van de Hulst, H. C., 1957: *Light Scattering by Small Particles*. John Wiley, 470 pp.

Waterman, P. C., 1965: Matrix formulation of electromagnetic scattering. *Proc. IEEE,* **53,** 805.

Wessels, H. R. A., 1972: Measurements of raindrops in De Bilt (in Dutch). KNMI Tech. Rep. WR-72-6, R. 41 pp.

Wexler, R., and D. Atlas, 1963: Radar reflectivity and attenuation of rain. *J. Appl. Meteor.,* **2,** 276–280.

Zinevich, A., P. Alpert, and H. Messer, 2008: Estimation of rainfall fields using commercial microwave communication networks of variable density. *Adv. Water Resour.,* **31,** 1470–1480.

——, H. Messer, and P. Alpert, 2009: Frontal rainfall observation by a commercial microwave communication network. *J. Appl. Meteor. Climatol.,* **48,** 1317–1334.